A&A 527, A98 (2011)
DOI: 10.1051/0004-6361/201015901

Astronomy & Astrophysics

The spectroscopic evolution of the symbiotic-like recurrent nova V407 Cygni during its 2010 outburst

I. The shock and its evolution

S. N. Shore[1,2], G. M. Wahlgren[3,4], T. Augusteijn[5], T. Liimets[5,6], K. L. Page[7], J. P. Osborne[7], A. P. Beardmore[7], P. Koubsky[8], M. Šlechta[8], and V. Votruba[8]

[1] Dipartimento di Fisica "Enrico Fermi", Università di Pisa, largo B. Pontecorvo 3, 56127 Pisa, Italy
e-mail: shore@df.unipi.it
[2] INFN – Sezione di Pisa, Italy
[3] The Catholic University of America, Dept. of Physics, 620 Michigan Ave NE, Washington DC, 20064, USA
e-mail: glenn.m.wahlgren@nasa.gov
[4] NASA-GSFC, Code 667, Greenbelt, MD, 20771, USA
[5] Nordic Optical Telescope, Apartado 474, E-38700 Santa Cruz de La Palma, Santa Cruz de Tenerife, Spain
e-mail: [tau;tiina]@not.iac.es
[6] Tartu Observatory, Tõravere 61602, Estonia
e-mail: sinope@aai.ee
[7] Dept. of Physics and Astronomy, University of Leicester, Leicester LE17RH, UK
e-mail: [apb;julo;kpa]@star.le.ac.uk
[8] Astronomical Institute, Academy of Sciences of the Czech Republic, 25165 Ondřejov, Czech Republic
e-mail: koubsky@sunstel.asu.cas.cz

Received 9 October 2010 / Accepted 29 November 2010

ABSTRACT

Context. V407 Cyg was, before 2010 Mar., known only as a D-type symbiotic binary system in which the Mira variable has a pulsation period of approximately 750 days, one of the longest known. On 2010 Mar. 10, it was discovered in outburst, eventually reaching $V < 8$. This is the first recorded nova event for this system, but it closely resembles the spectroscopic development of RS Oph, the prototypical symbiotic-like recurrent nova. It was also detected by *Fermi* above 100 MeV and displayed strong, likely nonthermal centimeter wavelength radio emission.

Aims. Unlike classical novae occurring in compact cataclysmic binary systems, for which the ejecta undergo free ballistic expansion, this explosion occurred within the dense, complex wind of a Mira variable companion. This paper concentrates on the development of the shock and its passage through the Mira wind. We also present some constraints on the binary system properties.

Methods. Using medium and high resolution ground-based optical spectra, visual and *Swift* UV photometry, and *Swift* X-ray spectrophotometry, we describe the behavior of the high-velocity profile evolution for this nova during its first three months.

Results. Using the diffuse interstellar bands visible in the high-resolution optical spectra, we obtain an extinction $E(B-V) \approx 0.45 \pm 0.05$. The spectral type of the red giant during this period, when the star was at R minimum, was no earlier than M7 III. The peak of the X-ray emission occurred at about day 40 with a broad maximum and decline after day 50. The main changes in the optical spectrum began at around that time. The He II 4686 Å line first appeared between days 7 and 14 and initially displayed a broad, symmetric profile that is characteristic of all species before day 60. The profile development thereafter depended on ionization state. Low-excitation lines remained comparatively narrow, with $v_{\rm rad,max}$ of order 200–400 km s^{-1}. They were systematically more symmetric than lines such as [Ca V], [Fe VII], [Fe X], and He II, all of which showed a sequence of profile changes going from symmetric to a blue wing similar to that of the low ionization species but with a red wing extended to as high as 600 km s^{-1}. The [O I] 6300, 6364 doublet showed a narrow wind-emission component near the rest velocity of the system and a broad component, 200–300 km s^{-1}, whose relative intensity increased in time. Forbidden lines of N II and O III had two separate contributors to the profiles, a broad line that increased in strength and velocity width, exceeding 200 km s^{-1}, and narrow components from a surrounding ionized region at higher velocity than the Mira wind. The Na I D doublet developed a broad component with similar velocity width to the other low-ionization species. The O VI Raman features observed in recent outbursts of RS Oph were not detected. We interpret these variations as aspherical expansion of the ejecta within the Mira wind. The blue side is from the shock penetrating into the wind while the red wing is from the low-density periphery. The maximum radial velocities obey power laws, $v_{\rm max} \sim t^{-n}$ with $n \approx 1/3$ for red wing and ≈0.8 for the blue.

Key words. novae, cataclysmic variables – stars: individual: V407 Cyg – stars: individual: RS Oph – binaries: symbiotic – galaxies: active

1. Introduction

The recurrent novae (RNe), the rarest and most extreme of the classical novae, are known in two distinct varieties (for a general series of overviews and specific details on observations and models see Bode & Evans 2008; Evans et al. 2008; Bode 2010). Both show repeated episodes of explosive mass ejection, between 10^{-7} $M_\odot$ and 10^{-6} $M_\odot$, on recurrence timescales of decades with velocities (based on the ultraviolet resonance

transitions) that can exceed 5000 km s^{-1}. One group is indistinguishable from classical novae: compact systems with orbital period <1 day and a low-mass (normally main-sequence) star that transfers mass to its companion white dwarf (WD) by Roche lobe overflow in a stream and accretion disk (Shaefer 2010). The other even rarer group, far less well studied but no less significant, resembles the symbiotic binaries, the so-called "symbiotic-like recurrent novae" (SyRNe), in which the mass-losing star is a red giant (RG) (e.g. Gonzalez-Riestra 1992; Anupama & Sethi 1994; Shore et al. 1996; Shore 2008; Anupama 2008; Schaefer 2010). Until this year, there were only four known in the Galaxy: V745 Sco, V3890 Sgr, RS Oph, and T CrB. Unlike the compact systems (e.g. U Sco), which have orbital periods coincident with classical cataclysmics, these systems have long orbital periods (years) and the WD likely accretes mass from the RG wind, instead of a stream. T CrB and RS Oph, for which accurate orbital parameters are known, host a WD whose mass exceeds that of the RG and for which the degenerate is more massive than in the symbiotic novae (not to be confused, these do not explosively eject mass and, instead, display a thermonuclear runaway that enters a long-term period of burning with an inflated WD envelope). The latter type are on the more active end of the symbiotic systems, the WD is the less massive component and $\leq 1\ M_{\odot}$.

Recurrent novae are produced by the initiation of a thermonuclear runaway provoked by accretion on massive WDs, which are nearer to the Chandrasekhar limit (for RS Oph, $M_{WD} \approx 1.2\ M_{\odot}$) than for normal symbiotics or symbiotic novae ($<1\ M_{\odot}$) (see Starrfield 2008; Anupama 2008; Mikolajewska 2008; Brandi et al. 2009). The connection of these systems, and their supersoft XR emission after outburst, to SN Ia progenitors has long been a scenario (e.g. Munari & Renzini 1992; Hernanz & José 2008; Sokoloski et al. 2006; Walder et al. 2008; Bode 2010; Schaefer 2010). The amount of mass that remains on the WD after the explosion is the critical determining factor. It is still unknown if there is a wind subsequent to the explosion that continues to remove the accreted mass, thus preventing the eventual critical accumulation to produce a collapse of the WD, or if the explosion ends abruptly and ejects only a fraction of the mass. However, no symbiotic had ever been observed to display a classical nova explosion until that of V407 Cyg. This is why the system is both unique and significant.

V407 Cyg, a D-type symbiotic binary with a long period Mira RG (Munari et al. 1990), underwent its first ever recorded explosive mass ejection on 2010 Mar. 10, reaching an unfiltered magnitude of 6.8 (Nishiyama & Kabashima 2010) and V magnitude peak of 7.9. Historically, V407 Cyg was first identified by its nova-like behavior in 1936 (Hoffmeister 1949; Meinunger 1966) in the $m_{\rm pg}$ range 14 to 16.5, but with identified contributions to the light curve from the Mira variable. Since that time, it has been observed to periodically increase in brightness according to the long-period Mira, and minor, slowly developing outbursts, never becoming brighter than approximately $V = 11.5$ during the years 1984–1995 (Kolotilov et al. 1998). A slow-developing outburst in the late 1990s was identified from the light curve (Kolotilov et al. 2003; Shugarov et al. 2007), as it was claimed to become brighter than the outburst of 1936, but never being brighter than $V \sim 11.8$. Large gaps in the light curve exist from the discovery data epoch until around 1990, which are of sufficient duration to have missed any outburst similar to the current event. Unfiltered optical monitoring of V407 Cyg during the two years prior to the March outburst shows a step-like brightness increase of nearly three magnitudes over a one year interval prior to outburst (Abdo et al. 2010). The 2010 outburst increased the brightness by an additional 2.5 mag. These step-like brightness increases, along with other irregular brightness variations, are vaguely present in the historical light curve.

Spectra from 2010 March 14-16, reported by C. Buil[1], showed very broad emission lines for all permitted transitions, especially the H Balmer lines, and He I, with an ejection velocity >2000 km s^{-1}, with superimposed very narrow emission lines. The surprise that V407 Cyg was previously considered a classical – although somewhat unusual – symbiotic was compounded by the high-energy detection of both X-rays (XR) and γ-rays above 100 MeV (Abdo et al. 2010). These were interpreted as the signature of π°-production by shock-energized protons in the RG wind during the first four days of the outburst, when the velocities exceeded 2000 km s^{-1}.

In this first paper we focus on the shock and its development. In subsequent papers we will present the analysis of the circumstellar material illuminated by the photoionization produced during the outburst and a line list constructed using high resolution spectra obtained from the Nordic Optical Telescope (NOT) on day 22 of the event, before the peak of the XR emission.

2. Observations

Our optical observational data set consists of spectra taken between 2010 Mar. 24 and 2010 Jul 16 with the Ondřejov Observatory Zeiss 2.0 m telescope coudé spectrograph and with the 2.6 m Nordic Optical Telescope (NOT) fiber-optic echelle spectrograph (FIES, program P40-423). The Ondřejov spectra taken with the SITe005 800 × 2000 chip were mainly obtained in the vicinity of Hα, supplemented by spectra at both bluer and redder wavelengths. The dispersion of 0.24 Å per pixel provided spectral coverage of approximately 500 Å, and exposure times ranged from 60 s to 6700 s. The FIES spectra were obtained with a dispersion of 0.023 Å px^{-1} in high-resolution mode covering the spectral interval from 3635 to 7364 Å and 0.035 Å px^{-1} in medium-resolution mode covering the spectral interval from 3680 to 7300 Å. Exposures ranged from 100 s to 3000 s. Absolute fluxes for the NOT spectra were obtained using the flux standard star BD +28°4211 observed on Jun. 3 and Jun. 23 at high resolution. Other spectra were not absolutely calibrated. All NOT spectra were reduced using IRAF, FIESTools, and our own special purpose routines written in IDL[2]. In several instances, contemporaneous spectra between the two observatories allow us to correlate and cross-calibrate the data. The journal of our observations is presented in Tables 1 and 2, which provides the observation start time in the systems Universal Time, Julian Date, JD, and ΔT, the approximate time since maximum optical light ($T0$). The $T0$ parameter has been adopted to be 2010 Mar. 10.813 = JD 2 455 266.313 (see Sect. 3.1) for XR analysis. For the journal of observations we adopt the value JD 2 455 266.30 as a guide to following the discussion, based on the three nearly coincident reportings of maximum brightness in CBET #2199.

[1] URL: http://www.astrosurf.com/~buil/v407cyg/obs.htm

[2] IRAF is distributed by the National Optical Astronomy Observatories, which are operated by the Association of Universities for Research in Astronomy, Inc., under cooperative agreement with the US National Science Foundation.

Table 1. Nordic optical telescope observations.

Spectrum ID	Date	UT	JD-240 000	ΔT (days)[a]	t_{exp} (s)	Object[b]
FItc310098	2010-04-01	05:28:24.8	55 287.72806	21.4	1000	V407 Cyg HR
FItd010076	2010-04-02	05:38:54.7	55 288.73536	22.4	125	V407 Cyg HR
FItd010077	2010-04-02	05:43:11.5	55 288.73833	22.4	400	V407 Cyg HR
FItd230110	2010-04-24	05:11:12.5	55 310.71612	44.4	1000	V407 Cyg HR
FItd270157	2010-04-28	05:30:37.4	55 314.72960	48.4	100	V407 Cyg HR
FItd270158	2010-04-28	05:33:40.3	55 314.73172	48.4	1000	V407 Cyg HR
FIte170040	2010-05-18	04:52:22.9	55 334.70304	68.4	4	V407 Cyg HR
FIte170041	2010-05-18	04:53:48.6	55 334.70403	68.4	100	V407 Cyg HR
FIte170042	2010-05-18	04:56:54.0	55 334.70615	68.4	1000	V407 Cyg HR
FIte260044	2010-05-27	04:38:28.8	55 343.69339	77.4	400	V407 Cyg HR
FIte260045	2010-05-27	04:46:30.5	55 343.69896	77.4	3000	V407 Cyg HR
FItf020080	2010-06-03	04:03:20.1	55 350.66898	84.4	200	V407 Cyg HR
FItf020081	2010-06-03	04:08:01.8	55 350.67224	84.4	2564	V407 Cyg HR
FItf020084	2010-06-03	04:57:26.2	55 350.70655	84.4	500	BD+28d4211 HR
FItf150084	2010-06-16	04:08:29.0	55 363.67256	97.4	200	V407 Cyg HR
FItf150085	2010-06-16	04:13:11.8	55 363.67583	97.4	3000	V407 Cyg HR
FItf220081	2010-06-23	03:10:23.3	55 370.63221	104.3	500	BD+28d4211 MR
FItf220083	2010-06-23	03:27:37.6	55 370.64419	104.3	270	V407 Cyg MR
FItf220084	2010-06-23	03:33:29.5	55 370.64826	104.3	2700	V407 Cyg MR
FItg150076	2010-07-16	00:00:52.9	55 393.50061	127.2	270	V407 Cyg MR
FItg150077	2010-07-16	00:06:44.7	55 393.50468	127.2	2700	V407 Cyg MR

Notes. [a] $T0$ (JD) = 2 455 266.30; [b] HR = high resolution, MR = moderate resolution.

3. Analysis

3.1. Swift observations: XRT and UVOT

Swift (see Gehrels et al. 2004) started observing V407 Cyg three days after the peak of the optical light-curve (2010 Mar. 10.813 = JD 2 455 266.313, hereafter denoted as $T0$), with both the X-ray Telescope (XRT, Burrows et al. 2005) and the UV/Optical Telescope (UVOT, Roming et al. 2005). Short observations (1 to 2 ks) were performed every few days until Apr. 2 ($T0$+23.1 days, JD 2 455 280, the start of our Ondřejov observations), at which point the exposure time was increased to ∼4 ks every other day (with a ∼10 ks observation on 2010 Apr. 17; $T0$+37.6 days). From 2010 Apr. 28 until May 6 (days 48.6–56.3), 3 ks were obtained every four days. From 2010 May 18 ($T0$ + 68.7 days), observations of about 1 ks were taken weekly until 2010 July 2.7. Data were processed using version 3.5 of the *Swift* software (released as part of HEASoft 6.8 on 2009 December 03) and the most up-to-date calibration files.

Initially the XRT PC mode count rate remained low, ∼0.01–0.02 count s^{-1} until $T0$ + 15.2 days. The rate started to increase at $T0$+12.4 days, reaching a peak of ∼0.26 count s^{-1} on $T0$+30.5 days. The X-rays then began a slow decay until around $T0$+56 days, at which point the count rate stopped decreasing, remaining between 0.08–0.09 count s^{-1}. The light curve is shown in Fig. 1.

The UV source was bright and most of the data were collected in the uvm2 filter (central wavelength 2246 Å); observations in u and uvw1 were saturated and are not shown. The initial data showed a slow decline (approximately 0.02 mag day^{-1}) that steepened to ∼0.09 mag day^{-1} around 40 days after peak; after $T0$+56 days the decay once more slowed to 0.05 mag day^{-1}. This reduced rate of decline in the UV light curve starts at around the same time as the XR flux stops declining, a similar feature appears in the AAVSO V band light curve at this time. As we discuss below, this is the same behavior derived from the optical emission lines and, in particular, from the third light continuum detected using the photospheric absorption lines from the Mira.

The XR spectrum remained relatively hard throughout the observations, with no strong emergence of super-soft emission. The hardness ratio (defined as the count rate ratio [1–10 keV]/[0.3–1 keV]) appears to soften until around day 30, after which time it remains approximately constant (see Fig. 1). Spectra were extracted before $T0$+30 days (as the XR light-curve was brightening), $T0$ = 30–60 days (as the X-rays were fading) and after day 60 (when the XR count rate was approximately constant). The earliest two spectra are very flat and cannot be fit with simple models; by χ^2 fitting we ruled out all solar abundance models from single-temperature optically-thin models with a single absorption component to two-temperature models with two absorption components, see Table 3. We used the Wilms et al. (2000) abundances and absorption model and the mekal plasma emission model. In contrast, non-solar abundance two-temperature models fit these two spectra well. For the late-time (after day 60) spectrum, only a single temperature component was needed; however, a non-solar abundance was still a significant improvement. We were able to achieve a good fit to all three spectra simultaneously, using the same abundances for each, but with other parameters taking different values. While two emission components were required for the spectra before day 60, we could not distinguish between a blackbody and an optically-thin plasma model for the lower temperature component. Both spectral components were absorbed by a single-component cold-absorption model, with the column density decreasing with time. The temperature of the hotter ($kT \approx$ 2–4 keV) component was also lower in the second spectrum, although the luminosity was unchanged. The (single) temperature of the spectrum extracted after day 60, when the XR count rate remained close to constant, was again lower, while the absorbing column was consistent with the day 30–60 spectrum. The luminosity of the low temperature component is not well constrained due to the combination of its low temperature and high absorbing column. The abundances implied by this fit are very high for N and O, abundances for elements other than those listed were fixed at solar. The simultaneous spectral fit had χ^2/d.o.f. = 480/383 (reduced χ^2 = 1.25)

Table 2. Ondřejov observations.

Spectrum ID	Date	UT	JD - 2 400 000.	ΔT (days)[a]	t_{exp} (s)	λ_{min} (Å)
tc230055	2010-03-24	01:45:46	55 279.57345	13.3	1641	6258
tc230056	2010-03-24	02:13:45	55 279.59288	13.3	373	6258
tc230058	2010-03-24	02:24:21	55 279.60024	13.3	447	6258
tc230059	2010-03-24	02:32:24	55 279.60583	13.3	389	6258
tc230060	2010-03-24	02:39:31	55 279.61078	13.3	360	6258
tc230065	2010-03-24	03:07:52	55 279.63046	13.3	328	8392
tc230066	2010-03-24	03:14:45	55 279.63524	13.3	1985	8392
td020076	2010-04-03	01:59:53	55 289.58325	23.3	577	6258
td020077	2010-04-03	02:10:07	55 289.59036	23.3	586	6258
td020078	2010-04-03	02: 20:32	55 289.59759	23.3	599	6258
td030034	2010-04-04	01:33:58	55 290.56525	24.3	541	6257
td030035	2010-04-04	01:43:38	55 290.57197	24.3	586	6257
td030036	2010-04-04	01:54:04	55 290.57921	24.3	626	6257
td050019	2010-04-06	00:35:32	55 292.52468	26.2	936	6257
td050022	2010-04-06	00:58:26	55 292.54058	26.2	3759	4753
td060048	2010-04-06	23:16:59	55 293.47013	27.2	1255	6257
td060055	2010-04-06	23:48:47	55 293.49221	27.2	6718	4797
td060063	2010-04-07	01:51:17	55 293.57728	27.3	1996	6400
td070033	2010-04-08	02:33:25	55 294.60654	28.3	60	6257
td070034	2010-04-08	02:35:58	55 294.60831	28.3	300	6257
td070037	2010-04-08	02:48:24	55 294.61694	28.3	60	8392
td070038	2010-04-08	02:50:52	55 294.61866	28.3	2000	8392
td210056	2010-04-22	02:37:40	55 308.60949	42.3	500	8395
td210057	2010-04-22	02:47:17	55 308.61617	42.3	500	6259
td260020	2010-04-26	23:12:42	55 313.46715	47.2	4135	6261
td260021	2010-04-27	00:25:59	55 313.51804	47.2	1106	6261
td280030	2010-04-28	23:37:32	55 315.48440	49.2	800	6260
td280036	2010-04-29	02:02:32	55 315.58509	49.3	1999	8396
tf040013	2010-06-04	23:06:20	55 352.46273	86.2	3000	6258
tf040020	2010-06-05	00:15:17	55 352.51061	86.2	300	8394
tf040022	2010-06-05	00:25:57	55 352.51802	86.2	2400	8394
tf040030	2010-06-05	01:19:26	55 352.55516	86.3	2000	7681
tf060016	2010-06-06	20:46:29	55 354.36561	88.1	4499	6260
tf070017	2010-06-07	20:35:33	55 355.35802	89.1	3000	6740
tf070021	2010-06-07	21:32:43	55 355.39772	89.1	3600	7246
tf070030	2010-06-07	23:31:08	55 355.47995	89.2	2100	6258
tf140016	2010-06-14	21:24:24	55 362.39194	96.1	3600	8393
tf140020	2010-06-14	22:32:02	55 362.43891	96.1	1800	6256
tg120015	2010-07-12	21:16:22	55 390.38637	124.1	3600	6259

Notes. [a] $\Delta T = T - T0$, with $T0$ (JD) = 2 455 266.30.

for the optically-thin plus blackbody model, and χ^2/d.o.f. = 489/385 (reduced χ^2 = 1.27) for the two-temperature optically-thin model. The results of the former fit are shown in Table 4 and Fig. 2; all errors and limits are at 90% confidence. The lower temperature component is responsible for 14% and 11% of the counts in the early and middle spectra, respectively. It remains possible that a yet more complex temperature distribution would reduce the implied high N abundance, although we were not able to find a sensible better fit with three temperature components. Consistent with the XRT spectral fits there is no detectable signal in the *Swift* BAT, with the 15 to 50 keV count rate remaining below 0.003 count cm^{-2} s^{-1}.

For both spectra, the luminosity at 2.7 kpc (Munari et al. 1990) is approximately 1.2×10^{34} erg s^{-1} for days 0–30 and 30–60. The day 60+ spectrum has a corresponding luminosity of about half this value, 6.4×10^{33} erg s^{-1}. This is the *unabsorbed* luminosity, for the *hotter* component* only. The final non-solar abundance enhancements tied between both spectra, with respect to Wilms et al. (2000) are N > 251, O = 35^{+30}_{-20}, Ne <3.1, Na = 103^{+103}_{-84}, and Mg < 2.3. The upper limit to the Ne and uncertain O abundances do not indicate an ONe white dwarf as the site of the explosion. They do not, however, exclude it since the ejecta rapidly mix with the environmental material (Walder et al. 2008) the abundances of which are closer to solar than expected from the nucleosynthesis occurring during the nova event. Thus, the final elemental mixture of the ejecta may be substantially altered during their passage through the Mira wind.

3.2. Interstellar extinction and spectral type of the Mira

The analysis of the bolometric properties of the explosion requires a determination of the reddening independent of the XR analysis. Using the colors of the Mira variable, and an assigned spectral type of M6 III, Munari et al. (1990) derived an extinction of $E(B - V)$ = 0.57. We have instead used optical diffuse interstellar band (DIB) identifications from Herbig (1975, 1988) and Jenniskens & Desert (1994). We used the calibrations for the DIBs given in the latter reference. Several are either blended with emission lines (e.g. 4428 Å) or too weak to be measured, but most of the important features are accessible. Our measurements are listed in Table 5, the uncertainty is ±5 mÅ. The resulting reddening is $E(B-V) = 0.45 \pm 0.09$ that is

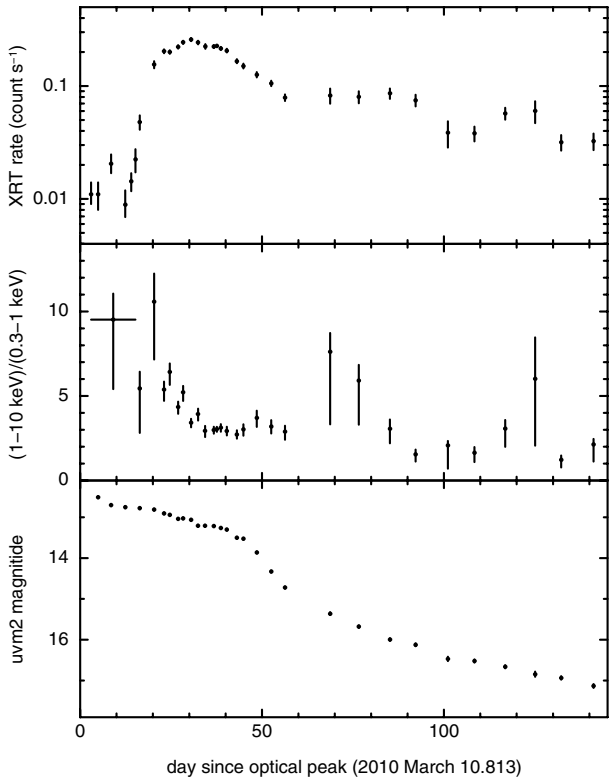

Fig. 1. *Swift* XRT 0.3–10 keV count rate, hardness ratio, and UVOT uvm2 (2246 Å) magnitudes of V407 Cyg as a function of time since the optical peak. For comparison with the optical spectroscopy, note that $T0$ = MJD 55266.

Table 3. χ^2/d.o.f. values for solar abundance models for the XRT spectra.

Model	χ^2/d.o.f.		
	<day 30	day 30–60	>day 60
mekal*tbabs	514/129	622/246	580/244
mekal*pcfabs	263/128	615/245	580/243
(mekal+mekal)*tbabs	210/127	476/244	430/242
(mekal+mekal)*pcfabs	208/126	301/243	414/241

consistent with but lower than the value derived from the energy distribution. We note, however, that the Mira was at minimum light during this outburst. We have compared the NOT spectra after MJD 55370 with those of giants in the range M 6–M 8 taken from the ESO/VLT/UVES *Library of High Resolution Spectra of Stars Across the H-R Diagram* archived data set (Bagnulo et al. 2003) and find that the present spectrum is a far better match to a later spectral type, close to M7 III or M8 III. In light of the approximate agreement of these different methods, we will adopt $E(B-V) = 0.5$ with a range of ±0.05.

Although there are no high resolution ultraviolet (UV) observations of V407 Cyg with which to independently check the interstellar medium along the line of sight, the O star HD 202347 lies at a close Galactic longitude and latitude. We show in Fig. 3 a comparison of the V407 Cyg Na I D line with interstellar S II 1259 Å resonance line in the STIS spectrum HD 202347, a B1 V star in NGC 7039. This is the closest OB star in Galactic longitude and latitude in the currently available UV archives[3]. The velocity also agrees with that of the nearby (line of sight) B8 II star HD 199206, $v_{\rm rad} = -21.0$ km s^{-1} from Wilson (1953)

[3] url: http://archive.stsci.edu/

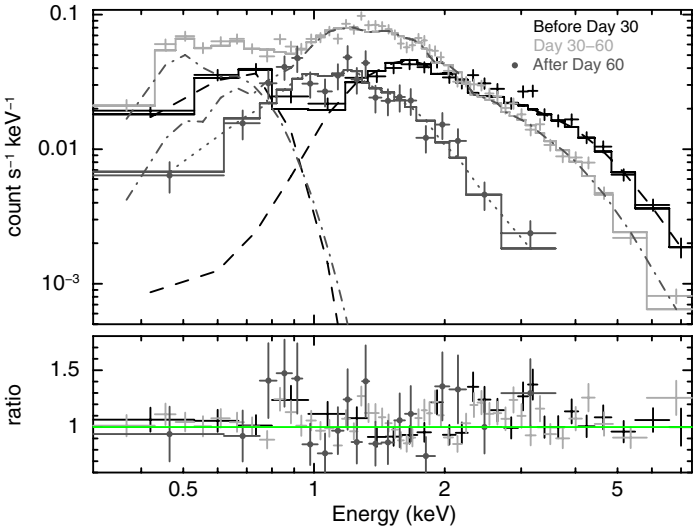

Fig. 2. The joint best fit to the *Swift* XRT spectra accumulated before day 30, from day 30 to day 60, and after day 60 from $T0$. The model is a strongly absorbed optically thin high temperature component with strongly enhanced nitrogen and oxygen *together with a lower temperature blackbody for the first two spectra*. See text for details.

Table 4. Best fit non-solar abundance models for the XRT spectra.

Day after $T0$	kT (BB) keV	kT (mekal) keV	$N_{\rm H}$ 10^{22} cm^{-2}	
<30	0.042±0.003	$4.10^{+0.67}_{-0.47}$	$1.55^{+0.14}_{-0.15}$	
30–60	$0.064^{+0.002}_{-0.004}$	$1.99^{+0.13}_{-0.12}$	0.62 ± 0.09	
>60	...	$0.80^{+0.16}_{-0.12}$	$0.69^{+0.11}_{-0.10}$	
Day after $T0$	Obs flux total	Unabs flux total	Obs flux hotter	Unabs hotter
<30	6.17E-12	2.44E-8	5.81E-12	1.09E-11
30–60	6.10E-12	6.99e-11	5.59E-12	1.17E-11
>60	1.34E-12	6.14E-12	1.34E-12	6.14E-12

Table 5. DIBs in the NOT spectrum of V407 Cyg, MJD 55288.

Wavelength (Å)	EW (m Å)	$E(B-V)$
5404	13	0.34
5780	234	0.49
6162	27	0.37
6379	29	0.37
6413	54	0.64
6623	109	0.47
6843	12	0.44

and DDO Radial Velocity Catalog. This clearly identifies the low velocity component in the V407 Cyg spectrum as interstellar and also shows that the higher velocity components are from the star, especially the wind and circumstellar material.

Several absorption lines, visible in the first NOT spectra, have been used to estimate the continuum contribution of the shock. These are from low-ionization resonance lines, known to be present in the quiescent spectrum and detected in the spectra of M6–M8 III stars. We show in Fig. 4 the comparison between the last NOT spectrum and stars from the ESO archive. The best match is to either M7 III or M8 III. The reported M6 III spectral classification of Munari et al. (1990) was obtained at a different phase ($0\overset{p}{.}1$, around maximum light) of the Mira while the 2010 outburst occurred at $0\overset{p}{.}6$ according to the Munari et al. ephemeris.

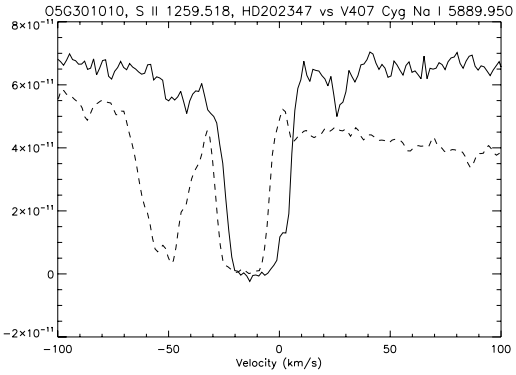

Fig. 3. Comparison of the Na I D1 profile of V407 Cyg (dash) with the S II 1257 Å resonance line in HD 202347 (solid, archival *HST*/STIS G140H spectrum, program O5G3), along a close line of sight. The high (negative) radial velocity components are from the Mira wind. The V407 Cyg spectrum, using the data from the first NOT observation, has been scaled for display; flux units for the *HST*/STIS spectrum are erg s^{-1} cm^{-2} Å^{-1}

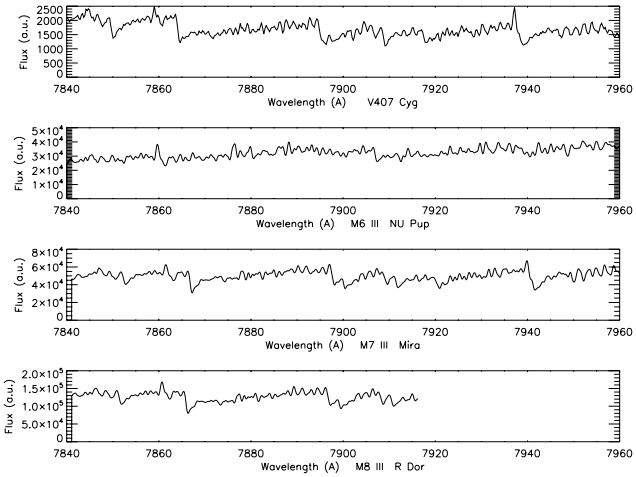

Fig. 4. Comparison of the Ondřejov spectrum from MJD 55358 with spectra for M6 III, M7 III, and M8 III stars from the ESO archive.

3.3. Low-ionization species

The O I emission features remained strong throughout the outburst but the line profiles show a complex structure. In the first NOT observation, the [O I] 6300, 6364 Å lines displayed very narrow central emission peaks, $FWHM = 12$ km s^{-1}, with low level, extended wings. The core emission remained nearly invariant while the broad wings increased throughout the observing interval to a maximum velocity of 200 km s^{-1}. This is shown in Fig. 5 from the NOT and Ondřejov sequences. The FWZI is nearly the same as the broad emission on the Na I D doublet, beginning at around the time of the break in the XR and UV emission seen in Fig. 1. The O I 8446 Å line is fluoresced by Lyβ through the O I 1027 Å resonance line (Bowen pumping), while [O I] 6300 Å is produced by recombination and cascade from absorption of the O I 1302 Å ground state transition, see Shore & Wahlgren (2010) for further discussion. The 8446 Å triplet narrowed during the interval from MJD 55279 ($v_{\rm rad,max} = -900$ km s^{-1}) to MJD 55315 (–400 km s^{-1}) after which it was unobservable in the Ondřejov spectra, being overwhelmed by photospheric absorption bands. We display in Fig. 6 the variations of the equivalent width for [O I] 6300 Å and O I 8446 Å. Note that the peak of the O I 8446 Å equivalent width is coincident with the XR peak and the increase of the [O I] 6300 coincides with the break in rate of decline of the UVOT fluxes and the 6700 Å continuum. The maximum velocity observed in the O I 8446 Å line is about 500 km s^{-1}. This suggests that the H I Lyβ pumped transition, O I 1025 Å, was as broad and was at its maximum at the XR peak or that the combined effects of ionization of the environmental Lyβ and the decrease of the intensity of the O I 1025 Å combined to produce the observed variation. No lines were detected for O II in the NOT spectra.

The [O III] 4959, 5007 Å forbidden lines showed identical profiles and were initially similar to [O III] 4363 Å. The 4363 Å line, however, never developed the double peak structure shown in Fig. 7, displaying only the broad component. This indicates two separate contributors to the nebular lines, one from material at comparatively large distance that has not been swept up by the shock with a mean density of 10^6 cm^{-3} for $T \approx 10$–20 kK, and the other, broader component with a density about a factor of 10 higher in the velocity interval consistent with impact of the ejecta.

The [N II] lines, in contrast, show the two narrow components on all three broad profiles (i.e. 5754, 6548, 6583 Å) although the latter two are invisible during the first three NOT observations due to overwhelming blending with Hα (see Fig. 7). They were, however, detectable in the Ondřejov spectrum taken on MJD 55308, at the peak of the XR emission. Their intensities increased relative to Hα by about a factor of 5 between MJD 55315 and MJD 55334 and the [N II] (6548+6583)/Hα ratio remained nearly constant after MJD 55352. The equivalent width ratio of [Ni II] 6667 Å to He I 6678 Å, which is independent of the extinction and absolute flux calibration, shows a behavior similar to that of the UVOT and 6700 Å continuum. The ratio steadily decreases throughout the outburst.

The [Ar III] 7135.79 Å line displayed the same profile as [N II] and [O III] 4959, 5007 Å, with two separate contributing regions. The photoionized region produced the same comparatively narrow emission peaks and the [O I] 6300 Å line has its maximum at the local minimum between the narrow line peaks at –67 and –29 km s^{-1}. The [Ar III] line, however, also developed a broad wing similar to [Ca V] (see below) extending from –200 to +300 km s^{-1} that contributed an approximately equal flux as the narrow lines. In contrast, [Ar IV] 4711 Å showed a similar profile to that of [Ca V] and He II but its peak is shifted in all spectra to +110 km s^{-1} (see below, Sects. 3.4 and 3.6).

The Ca II IR triplet (8498, 8542, 8662 Å) lines all showed broad wings from the earliest Ondřejov spectra, extending to 200 km s^{-1} (Fig. 8). There were several narrower emission peaks in all profiles at the same velocity as the Na I D absorption components. In contrast, the [Ca II] 7291, 7323 Å lines remained extremely narrow, compatible with the [O I] 6300 Å core (12 km s^{-1}), and never developed the broad wings that are seen on the Ca II 3968 Å resonance line or the fluoresced O I lines (Fig. 9). The Ca II lines showed two very different developments during the outburst. The 8498, 8542, 8662 Å triplet displayed a broad profile in the first observations that systematically narrowed throughout the observing interval, similar to O I 8446 Å. In contrast, the Ca II 7291, 7323 Å doublet remained narrow, ≈10 km s^{-1} ($FWHM$), and centered on the Mira, and never displayed broad wings.

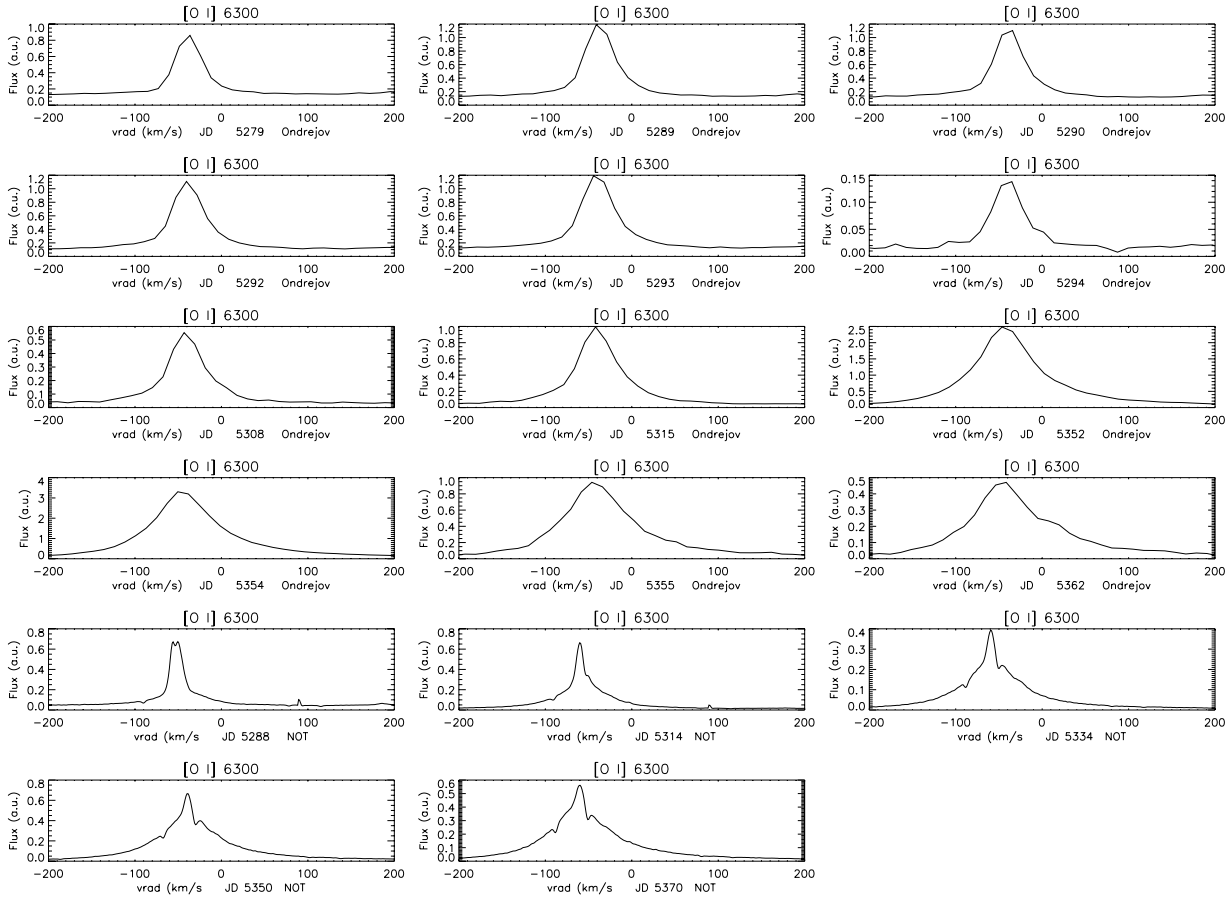

Fig. 5. Variation of the [O I] 6300 Å line profile from the Ondřejov (11.4 km s^{-1}px^{-1}) and NOT (1.1 km s^{-1} px^{-1}) data sets during the observing period. The date is a JD-2 450 000; the peak of the XR emission, around day 30, corresponds to JD 2 455 296.

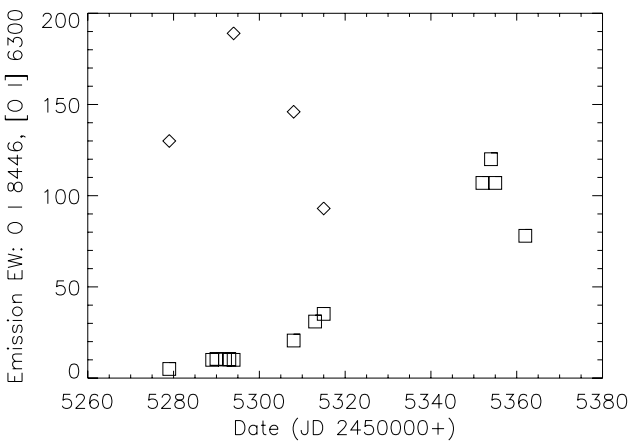

Fig. 6. Variation of the [O I] 6300 Å (open squares) and O I 8446 Å (open diamonds) equivalent widths during the outburst based on the Ondřejov spectra.

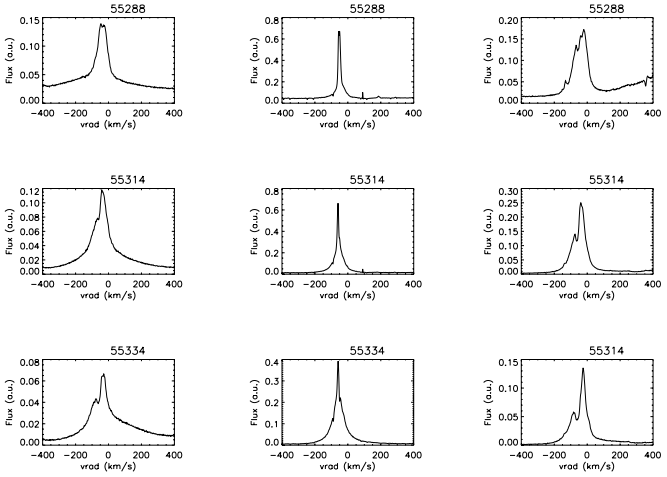

Fig. 7. Comparative development of low ionization species line profiles: [N II] 5754 Å (*left column*), [O I] 6300 Å (*center*), and [O III] 5007 Å (*right*) from NOT spectra on the three indicated dates during the outburst.

The Na I D lines displayed a broad component on which were superimposed the narrow absorption features (both ambient and interstellar, see below), extending to 150 km s^{-1}. The broad component increased steadily in strength throughout the observing interval, with the greatest change occurring after XR maximum. The centroid of the broad line appears to be shifted by about –16 km s^{-1} relative to the Mira but this may be an artifact of the fitting of a symmetric function (Gaussian) to what may be an intrinsically asymmetric profile of the same form as He II or [Ca V]. In Fig. 10 we show the Gaussian profiles for the two indicated epochs. The gallery of line profiles in Fig. 24 (see Sect. 3.7) shows the changes in the broad component

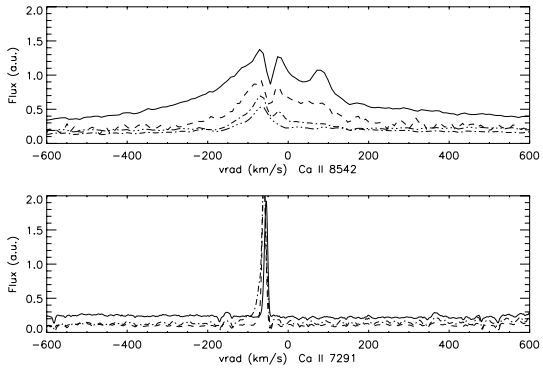

Fig. 8. *Top*: variation of the main line of the infrared Ca II triplet 8542 Å; solid: MJD 55279, dash: 55294, dot-dash: 55315, dot-dot-dash: 55362 (Ondřejov spectra). *Bottom*: comparison with Ca II 7291; solid: 55289, dash: 55314, dot-dash: 55363 (NOT spectra).

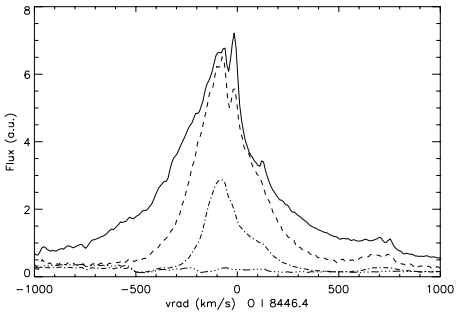

Fig. 9. Variation of Bowen fluorescence O I 8446 Å line for the same epochs as Fig. 8 (Ondřejov spectra).

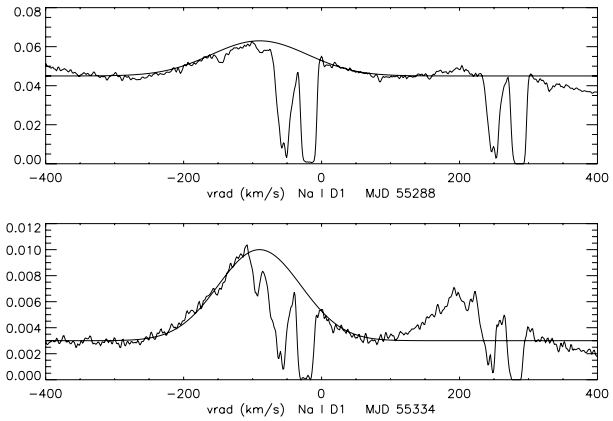

Fig. 10. Gaussian line profiles fit to the Na I D1 profile of the NOT sequence on the dates indicated. The line *FWHM* is 110 km s^{-1} for both and the centroid is displaced to –70 km s^{-1}.

width (along with the narrow circumstellar absorption and emission features).

The Mg I 4571 Å profile consisted of two components, like O I and [O I]: a narrow feature coincident with the Mira rest frame and broad wings extending from –200 to +100 km s^{-1} in the first NOT spectra. The line never displayed a P Cyg component or any of the absorption features observed on the Na I D lines. It strengthened during the outburst while remaining constant in velocity width. In Fig. 11 we show the variation of the [O I] 6300 Å and Mg I lines corrected for interstellar reddening.

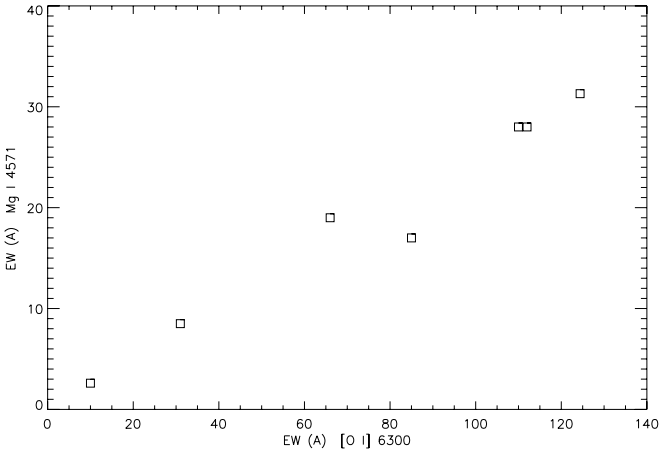

Fig. 11. O I 6300 Å equivalent width variations relative to Mg I 4571 Å with a reddening correction $E(B-V) = 0.5$ applied to the continuum.

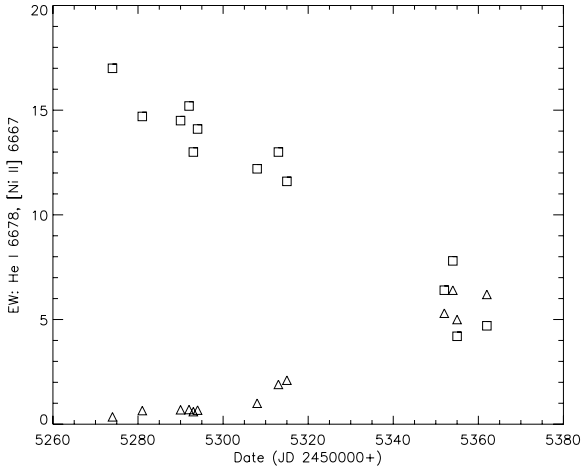

Fig. 12. Equivalent width variation of He I 6678 Å singlet (squares) relative to [Ni II] 6667 Å (triangles).

The equivalent variations of the [Ni II] 6667 Å line relative to the nearly adjacent He I singlet 6678 Å is shown Fig. 12. This comparison is unaffected by either reddening uncertainties or continuum variations. The He I line systematically decreased during the observing interval. In contrast, the [Ni II] 6667 Å line increased in equivalent with showing a change in rate of increase at around MJD 55300 similar to that seen for [O I] 6300 Å (e.g. Fig. 6) and [S II] 6730 Å (see below, Fig. 26).

We will present a detailed study of the variations of the Fe-peak neutral and singly-ionized species in the next paper (in preparation). However, for illustration and comparison with the other neutral and low ionization species, we show in Fig. 13 the P Cyg profiles observed on the narrow components of the Fe II RMT 42 lines observable in the NOT spectra. The absorption persisted throughout the outburst, even as the wings of the profiles increased in maximum radial velocity to 200 km s^{-1}. The profiles were asymmetric at first, with extended *blueward* wings, becoming more symmetric in later spectra. The broad wings are clearly from the shock while the narrow componwent – and the P Cyg absorption – is from the Mira wind and chromosphere.

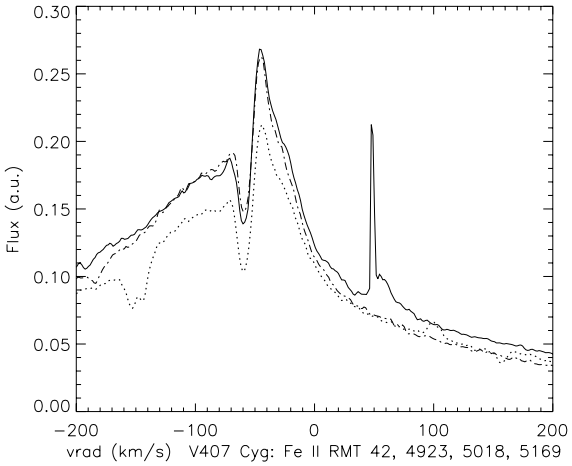

Fig. 13. Low velocity P Cyg absorption on the principal lines of Fe II RMT 42 4923 Å (solid), 5018 Å (dot-dash), 5169 Å (dot) on MJD 55286, before the peak of the XR emission. Note also the blueward extension of the line profiles (not shown beyond –200 km s^{-1}).

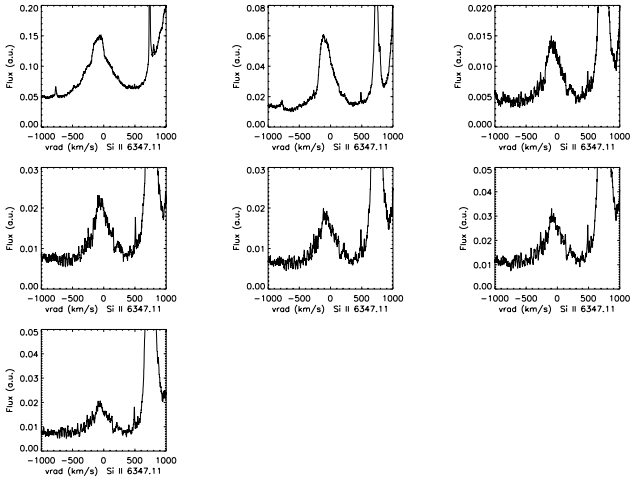

Fig. 14. Variation of Si II 6347 Å line profile in the NOT sequence. The first spectrum has a contamination from Hα that affects adjacent orders from the extreme saturation of the profile. This changes the core from –150 to +150 km s^{-1} but has no effect on the extended wings.

The Si II 6347 Å line displayed a broad profile throughout the observing interval with wings extending to nearly 400 km s^{-1} and no P Cyg structure at any time. The companion line at 6371 Å was always blended with Fe II 6369.37, 6371.13 Å and was unmeasurable. The profile was very different from the Ca II IR triplet, never showing either the multiple emission features or a strong asymmetry. The Si II 5041, 5056 Å lines showed broad profiles throughout the observing interval but these are composite, complex blends with [Fe II] 5039, 5043, 5060 Å. In the first NOT spectrum, however, they are dominated by Si II for which we obtain the central velocities are both –90 ± 10 km s^{-1} and $FWHM$ of 300 ± 18 km s^{-1} from Gaussian fitting. The lines were nearly of equal strength, and $v_{\rm rad,max}$ was ±400 km s^{-1}. The subsequent line profiles are too complex to permit such a characterization. Note that the displacement and line width is similar to that of the Na I D broad components. The line profiles are shown in Figs. 14 and 15. The comparison to He I 6678 Å, the only strong singlet observed in the outburst, shows the strong similarity in the profile and evolution.

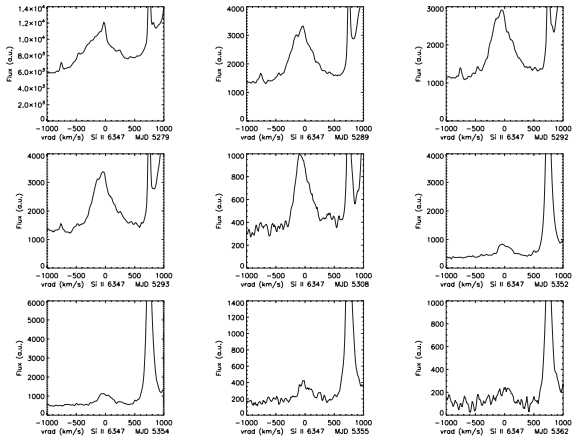

Fig. 15. Variation of Si II 6347 Å in the Ondřejov sequence. Compare this with Fig. 17 for He I 6678 Å. The profiles are unaffected by the contamination present in the NOT echelle spectra at any epoch.

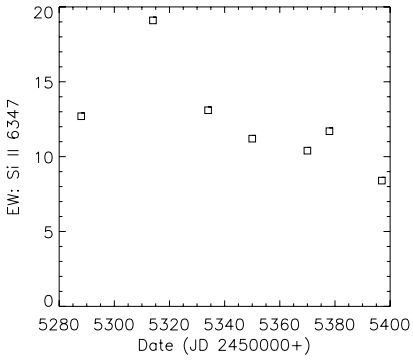

Fig. 16. Variation of Si II 6347 Å equivalent width from the NOT spectra. The peak in the emission occurs just after XR maximum.

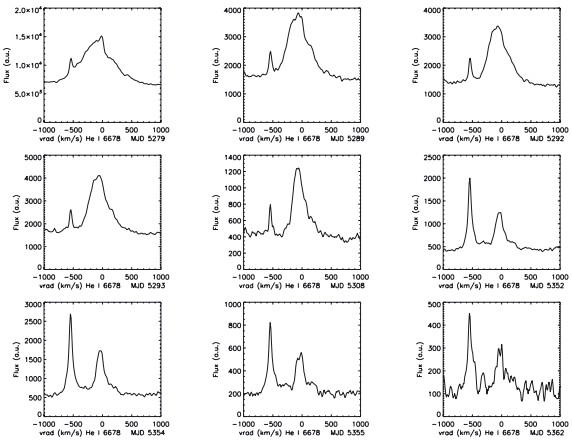

Fig. 17. Variation of He I 6678 Å in the Ondřejov sequence for comparison with the Si II 6347 Å profile evolution.

The He I line profile variations are shown in Figs. 17 and 18. Except for 6678 Å, *no* singlet line of neutral helium was observed. The profiles of the 6678 Å line, and those of the triplet series, evolved similarly. The first NOT spectrum displays a broad (nearly ±500 km s^{-1}), nearly symmetric profiles for the triplets and 6678 Å, but the subsequent development is different. The 6678 Å profile narrows but remains symmetric while the triplet lines develop multiple narrow emission features and an asymmetric shape extending from –200 to +500 km s^{-1}. The

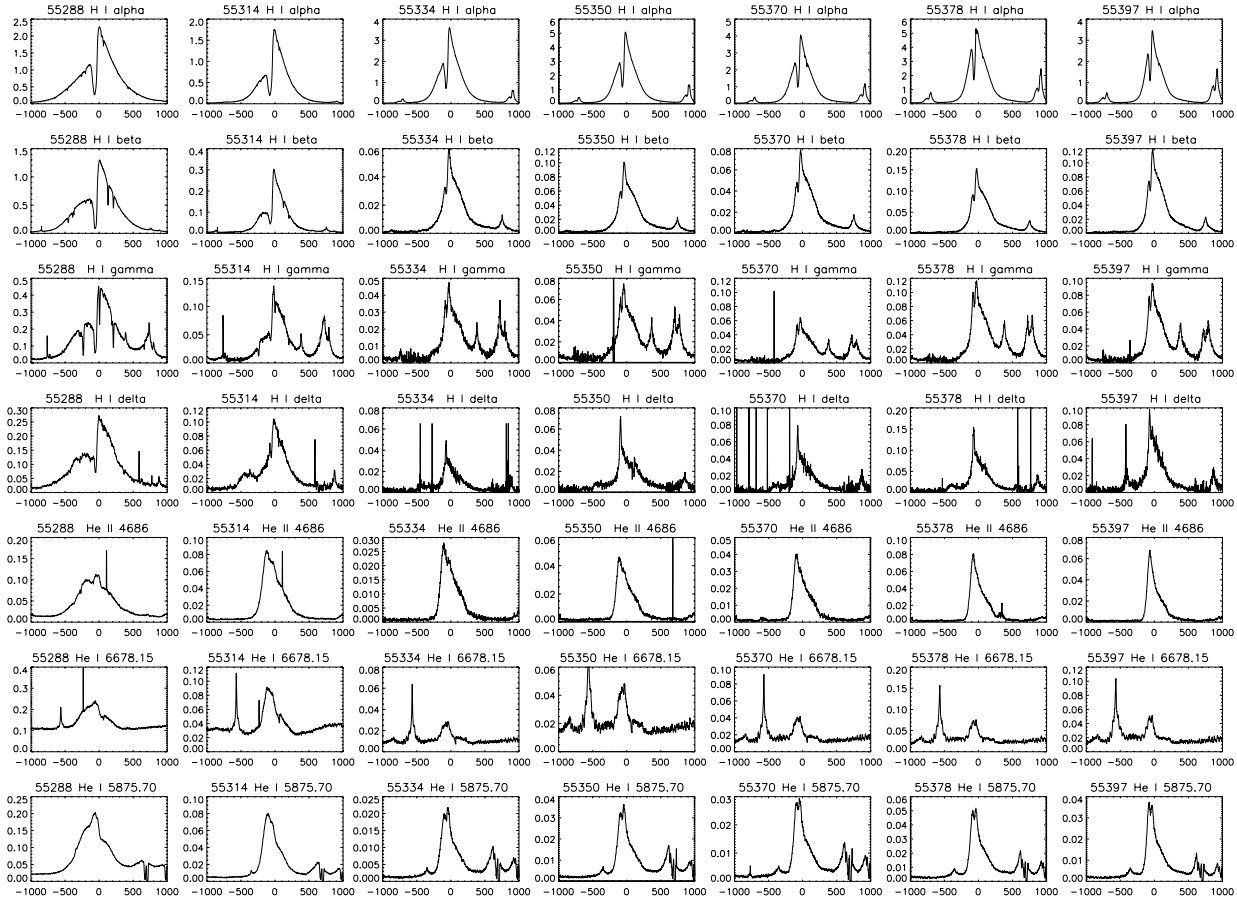

Fig. 18. Line profiles for H I Balmer Hα, Hβ, Hγ, and Hδ; He II 4686 Å; He I 6678 Å (singlet) and 5875 Å (triplet) for all NOT observations. The abscissa is uniformly radial velocity in km s^{-1}, the individual lines and MJD are indicated in the heading of each panel. The ordinate is flux in arbitrary units.

minimum at the peak of the lines corresponds precisely to the maximum of the narrow [O I] 6300 Å emission, as found for [N II] and [O III].

The He I line profiles developed very differently than during the 2006 RS Oph outburst. In the series shown in Fig. 51 of Iijima (2009), in the first week of the RS Oph outburst the profile showed a nearly triangular shape with wings extending to >1500 km s^{-1}, accompanied by narrower emission peaks at –200 and +100 km s^{-1}, that had narrowed to 800 km s^{-1} by day 35. The subsequent evolution is close to a power law with $v_{\rm rad,max} \approx -800(t/35)^{-1}$ km s^{-1} and similarly for the red wing. For V407 Cyg, the He I and He II line profiles varied similarly except that the 5875 Å line showed two narrow emission components at the line peak centered on the velocity of the Mira. The He II profile in RS Oph, from Fig. 50 in Iijima (2009), displayed multiple components throughout the outburst after day 35 and its broad wings remained symmetric, in contrast to V407 Cyg. As in V407 Cyg, the singlets were weak or absent in RS Oph 2006. Only narrow components are reported for any singlet, e.g. 4921 Å. The He I 6678, 7065 Å lines in RS Oph decreased steadily in time while remaining nearly constant relative to Hβ, the same was observed for V407 Cyg.

3.4. H I Balmer line profiles

The gallery of NOT spectra for the Balmer lines is shown in Fig. 18. The maximum velocity reported for the first Balmer line profiles (Mar. 14 = MJD 55269, C. Buil, priv. comm.) was >2500 km s^{-1} for Hα and Hβ. The first Ondřejov observation, (Mar. 25, MJD 55280) shows, instead, extended emission to 4000 km s^{-1}. This measurement is consistent with the Mar. 14 spectrum since the highest velocity is only seen in very weak wings (the S/N ratio for the first Ondřejov Hα profile is about 60 pix^{-1} at 4000 km s^{-1} and >1000 at line peak). The profiles show a low velocity P Cyg absorption that remains strong throughout the period covered by these observations for the Balmer α through γ lines, at –54 km s^{-1}. This is consistent with the rest velocity determined from the Li I 6707 Å and Ba II 4554 Å resonance lines. Weaker absorption lines of metallic species seen on the Balmer profiles, especially on Hβ, decreased systematically until MJD 55332, after which they are not detectable. The Hδ P Cyg trough at low velocity decreased systematically and turned into emission around the date of the UVOT light-curve descent.

Figure 19 shows the measured extreme radial velocities for the Hα, Hβ, and Hγ profiles. Blending prevented measurement of the extreme of the red wing of Hγ and the low signal-to-noise ratio at Hδ made the measurements unreliable. The uncertainties are ±20 km s^{-1} based on the continuum fitting. These should be compared with the He II 4686 Å measurements shown below in Fig. 26.

3.5. Li I 6707 Å and non-photospheric continuum emission

The Li I 6707 Å line was visible from the first spectrum for which we measured an equivalent width, W_λ = 42 ± 5m Å.

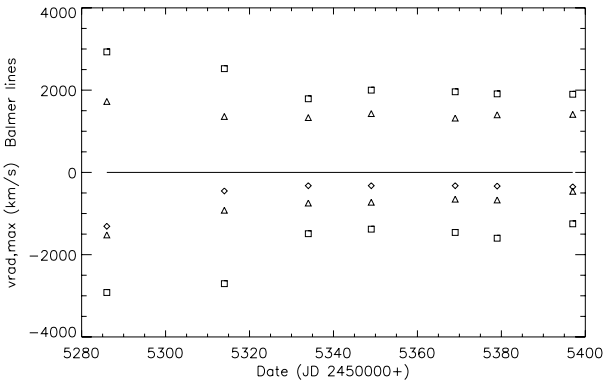

Fig. 19. Maximum radial velocity variation for the Balmer lines from the NOT spectra. Square: Hα, triangle: Hβ, diamond, Hγ.

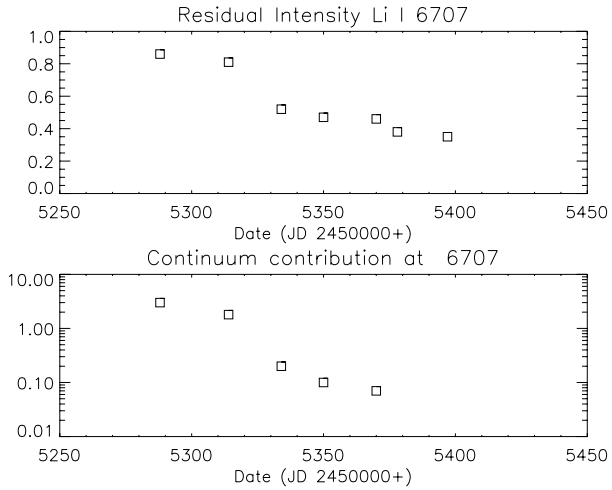

Fig. 20. Li I 6707-derived continuum contribution during the outburst, based on NOT spectra.

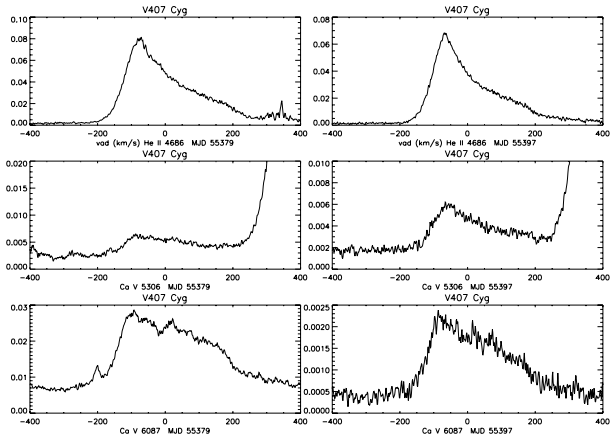

Fig. 21. The changes in line profiles for He II 4686 (*top*), [Ca V] 5308 Å (*middle*), and [Ca V] 6087 Å (*bottom*) on the last two NOT observations. The similarity of the two sets of profiles demonstrates that the asymmetry is a dynamical effect and not an optical depth effect (see text).

The evolution of the line indicates that it was not formed in the wind but, instead, is the photospheric absorption feature previously reported by Tatarnikova et al. (2003a,b), who reported W_λ = 350 m Å. Its radial velocity, –54 km s^{-1}, is consistent with the Mira being at minimum light. During the first two months, the line steadily increased until, after MJD 55350, it stayed constant. For the last two NOT spectra (medium resolution; MJD 55370, 55393) we obtained an equivalent width of 350 ± 10 m Å. If we assume the absorption line strength was, in fact, constant throughout the outburst, then the change was due to a "contamination" by a masking continuum; thus the additional continuum accounted for ≈90% of the light at 6700 Å during the earliest observation (MJD 55286) and is consistent with the observed decrease of 3 mag in R during the interval. This is consistent with the simultaneous increase in the atomic and molecular absorption line spectra longward of 6700 Å, with the gradual approach to the pre-outburst spectrum shown in Munari et al. (1990). The measurements are shown in Fig. 20. As we will discuss in Sect. 4, we interpret this continuum as probably being due to thermal bremsstrahlung emission from the shock.

3.6. High-ionization species

Shortly after the detection of γ-ray emission by *Fermi*, Munari et al. (2010) reported the presence of high-ionization species in the optical spectrum. Our NOT sequence, covering the same period at higher resolution, allows us to confirm several of the identifications. The [Fe X] 6375 Å line was present on the first Ondřejov spectrum (Mar. 25) and continued to increase in strength through May. After the XR peak, it rapidly declined while maintaining the same line profile, almost identical to He II 4686 Å. The line, initially nearly symmetric with maximum velocity of ∼500 km s^{-1}, became progressively more asymmetric in the same manner as the helium lines and virtually disappeared by Jun. 2. The [Ca V] lines, in contrast, remained visible throughout the observing interval and increased in strength through the XR peak, after which they declined less rapidly than [Fe X]. For [Ar X] 5535 Å, the detection is ambiguous because of the presence of a set of strong permitted Fe-peak lines superimposed on a broad but weak emission. The line is likely present in the first NOT spectrum.

Broad emission was first observed as early as Mar. 25. Munari et al. (2010) report the first detection of [Fe X] on Mar. 17, only one week after outburst, with a $FWHM$ of about 600 km s^{-1}. This contrasts with Iijima (2009) who reports, for the 2006 outburst of RS Oph, that [Fe X] and [Fe XIV] appeared only after day 35. [Fe X] 6375 Å showed a nearly symmetric profile before and at XR maximum, while [Ar IV] 4711 Å displayed a He II-like profile with an extended blue wing with a blueward maximum $v_{\rm rad}$ = −150 km s^{-1} in the stellar reference frame, [Fe X] 6375 Å extended from −400 to +600 km s^{-1}. This difference in the profiles persisted, the maximum blueward extension of [Fe X] was always greater than [Ar IV]. The [Ca V] 5309, 6086 Å lines were strong and showed a He II-like profile. These are compared in Figs. 21 and 24. [Ne IV] 4714, 4720 Å and [Fe XIV] 5303 Å were absent. The feature observed near [Ar X] 5533 Å is more likely an Fe II permitted line, based on its profile in the first NOT spectrum and no other [Ar X] line was detected.

Figure 22 shows the [Fe VII] line evolution in the NOT sequence and in Fig. 23, the last three epochs are compared to a simple model. The profile was computed using a spherical expansion Monte Carlo method described in Shore et al. (1994). The maximum velocity was fixed to 400 km s^{-1}, consistent with the He II line blue wing, and a ballistic velocity law was used. The only adjustment required is to shift the line centroid to +70 km s^{-1}. The best agreement was achieved with a fractional

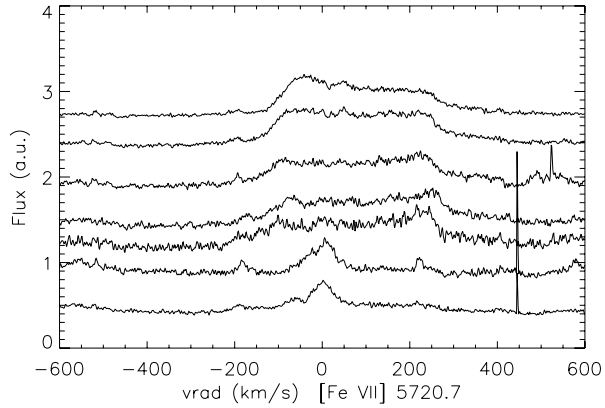

Fig. 22. Time development of [Fe VII] 5720 Å in the NOT spectra, from bottom to top in the same sequence shown in Fig. 24.

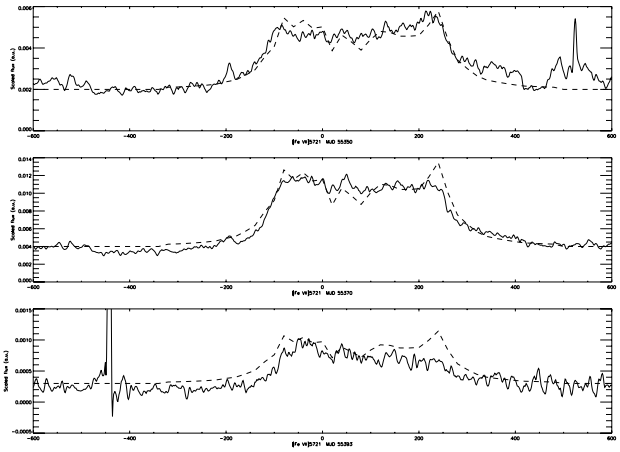

Fig. 23. The observed [Fe VII] 5720 Å line profiles (from MJD 55363, 55370, 5593) compared with the simulation described in the text.

thickness, $\Delta R/R = 0.6 \pm 0.2$. The model reproduces the profile best in the two earliest stages, during the initial deceleration of the ejecta, while the last shows an asymmetry on the red wing, likely due to a change in the emission measure of the lower density gas with respect to that of the approaching side of the shock in the denser wind of the Mira.

3.6.1. O VI Raman line profiles

The broad emission features 6825 Å and 7080 Å present in many symbiotics are Raman scattering lines of O VI, formed by the conversion to long wavelength of O VI 1032, 1037 Å doublet photons by the nearby Lyβ 1025 Å line (Schmid 1996; Schmid et al. 1999). Although the UV flux was several orders of magnitude greater than a normal symbiotic star and the ionization was sufficient to produce the O VI FUV doublet, no O VI Raman emission was detected at either spectral region during the time interval covered by these observations. This contrasts with the RS Oph 2006 outburst during which the 6825 Å line was detected (Brandi et al. 2009; Iijima 2009) in the early stages after outburst (before day 60). Brandi et al. note that the line was absent in quiescence. Our non-detection may be due to the orbital phase at which the eruption occurred. If the WD was at superior conjunction, the part of the Mira wind in which the O VI conversion occurred may have been occulted. In addition, unlike RS Oph 2006, at the time when recombination yielded sufficient column densities in Lyβ to produce the Raman scattering, after Jun. 3, the long wavelength region of the optical spectrum was dominated by the photospheric spectrum of the Mira.

3.7. Emission line flaring: Na I 5889, 5895 Å and [S II] 6716, 6730 Å

The absorption line evolution of the Na I D lines has been discussed recently for the circumstellar environment of several supernovae (Patat et al. 2007; Simon et al. 2009). We observed a systematic evolution of the absorption of several components during the post-outburst interval. In the first spectrum (MJD 55287), there is a very weak feature at –95 km s^{-1} with $W_\lambda = 5 \pm 1$m Å. Other absorption components were at –63, –59, and –54 km s^{-1}. These latter remained virtually unchanged throughout the entire sequence and we checked the variations relative to the interstellar absorption feature at –23 km s^{-1}. No variations greater than 10% were measured. Instead, the -95 km s^{-1} feature systematically grew in equivalent width, reaching a maximum in our last NOT observation (MJD 55393) of 120 ± 2 m Å. At the same time, we noted the increase in an *emission* line at +6 km s^{-1} that lagged the increase in the absorption by approximately two weeks. The sequence of line profiles is shown in Fig. 24.

We propose that this is the *rear* side of the same shell that is responsible for the absorption at –95 km s^{-1}, and that the delay measures the light-travel time across the structure. Assuming the measured velocity (in the absence of a dynamical model for the origin of the shell), the delay corresponds to a distance of approximately 4×10^{-3} pc (≈900 AU) and a tentative time of origin of about one century ago. This is relatively close to the epoch of the 1936 "novalike" event reported by Hoffmeister that has been responsible for the denomination "nova" for V407 Cyg in the subsequent literature (a misreading of the catalog entry). However, it is well known that symbiotic stars undergo outbursts, presumably thermonuclear runaways, during which time the degenerate mass accreter develops a strong wind. If this happened in the extended outburst in the 1930s, then we may be seeing that ejection through the Na I variations. The timescale for the increase in the absorption line then suggests an electron density of about 6×10^5 cm^{-3} at that distance. Without knowing the thickness of the shell, we can nonetheless estimate the mass-loss rate using the column density, finding for this component $\dot{M} \approx 4 \times 10^{-6}\ M_\odot$ yr^{-1}. Since the 1936 event lasted nearly a decade, this amounts to a comparatively low mass of about $10^{-4}\ M_\odot$, of which at least some part must be dust.

The [S II] 6716, 6730 Å lines displayed a different profile toward the end of the sequence than the first, narrow profiles with a centroid velocity of –60 km s^{-1}, hence very low velocity with respect to the star, spanning –150 to +50 km s^{-1}. They remained centered near the stellar velocity and never displayed the redward extension of the higher ionization lines. A curious feature of their late time evolution is an apparent flare (see Fig. 26) after MJD 55350 during which time the profile did not change. Flares of other low ionization species have been noted in Iijima (2009) for the RS Oph 2006 event. This is more consistent with a change in the ionization state of the medium than an impact of the shock. In fact, it appears that the [S II] 6716, 6730 doublet was not formed in the shock but rather in the Mira, near the base of the wind. It indicates, however, the interval over which the other high ionization species are "contaminated" by environmental emission. In particular, the peak of the He II line is partly

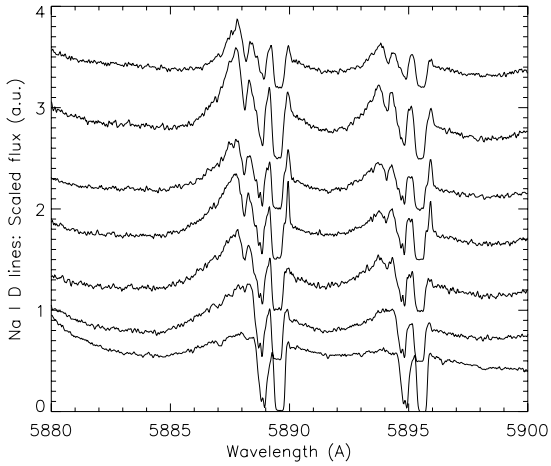

Fig. 24. Evolution of the Na I D doublet during the outburst (proceeds from bottom to top) from the NOT spectra. The spectra have been normalized for display. Note the appearance of the absorption on both components of the doublet at 5887.9 and 5894.6 Å and the narrow emission at 5890.0 and 5896.7 Å. See text for discussion.

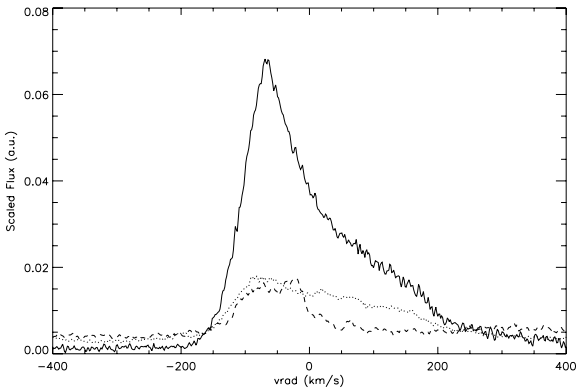

Fig. 25. Comparison between [S II] 6730 Å (dash), [Ca V] 6087 Å (dot), and He II 4686 Å (continuous) line profiles at the last NOT observation, MJD 55397. Note that the [S II] lacks the redshifted wing present on the higher excitation lines (see text for discussion).

contributed by the low velocity broad emission and this accounts e.g. for the difference between it and the [Ca V] and [Fe X] profiles.

4. Discussion: Toward a model of the outburst and the binary system

The 1985 and 2006 eruptions of RS Oph are the only symbiotic-like recurrent novae that have been followed throughout the event with modern, multiwavelength methods, and it is that system with which we will compare the 2010 V407 Cyg event. The optical light curves (see the supplementary material in Abdo et al. 2010) are almost identical although with different timescales, the V407 Cyg event was faster at all wavelengths. Although the spectroscopic development of the outburst was similar to that of the 1985 and 2006 events in RS Oph (Evans et al. 2008; Iijima 2009) there were some important differences. The maximum Balmer line velocity reached for V407 Cyg never exceeded 3000 km s^{-1} during the earliest stages of the

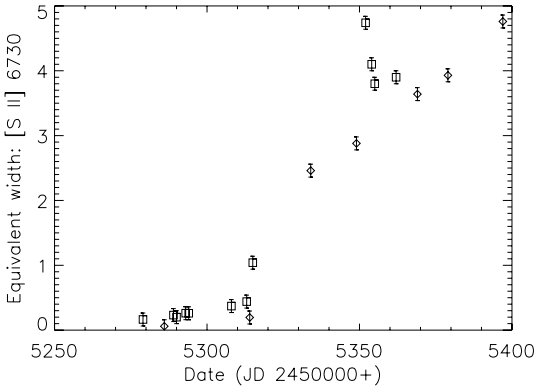

Fig. 26. Variation of the [S II] 6730 Å equivalent with showing the shortlived "flare" event at about day 84 of the outburst. There was no profile change during this increase. Square: Ondřejov spectra, diamond: NOT spectra. Note the rapid increase in line strength approximately coincident with the peak and initial decline of the XR emission (see Fig. 1).

expansion while those for RS Oph were well in excess of 4000 km s^{-1}. The Balmer line profiles were also systematically different, being more nearly broad Gaussians in V407 Cyg and nearly power laws in RS Oph (Anupama & Prabhu 1989; Iijima 2009). While the line structure has been interpreted as individual emission regions, the V407 Cyg variations show that the low velocity P Cyg profile at around –90 km s^{-1} is absorption that changes to emission late in the outburst (particularly evident on the Hδ line). The persistence of the P Cyg absorption on both the Hα, Hβ, Hγ, and Fe II (permitted) lines at low velocity (around +10 km s^{-1} in the system frame) is similar to that in the RS Oph 1985 and 2006 outbursts. A difference is the switch to emission at the same wavelength for Hδ at around the peak of the XR emission. The absorption was at the same velocity as the persistent narrow emission on the O I lines, particularly the forbidden transitions.

The extra continuum contribution derived using the Li I profile shows the same variation as the UVOT light curve. Scaling to the last date, Day 131 of the outburst, on which the contribution is about 10% of the photospheric continuum, and using the change in the Ba II 4554 Å line give a continuum consistent with bremsstrahlung assuming $E(B-V) = 0.5$. On MJD 55363 (day 104), for which we have a standard star calibration, the photospheric flux at 6705 Å, near Li I, was 1.6×10^{-14} erg s^{-1} cm^{-2} Å^{-1}. At maximum, in the first NOT spectrum, the extra continuum contributed a factor of ≈10 times higher (Fig. 20, bottom) at a time when the shock temperature from the XR mekal fit was $\approx 2 \times 10^7$ K, implying a velocity for the shock of ≈800 km s^{-1} for the interval from 30 to 60 days after $T0$. This is close to the measured maximum velocity on the Balmer and He II 4686 Å lines at the epoch of the first two NOT observations. The shock could then have powered the high ionization emission with the optical continuum being contributed by cooler gas behind the expanding front, consistent with the emission from the lower ionization lines. This is also sufficient to produce the strong precursor that is required to account for the rapid appearance of the high ionization narrow components. The decrease in H I column density can be explained by the passage of the shock through the wind and the decrease in neutral absorber due to photoionization (see also Shore et al. 1996).

The changes in the He I, He II, [Ca V], and Balmer line profiles require an aspherical shock, the blueshifted side

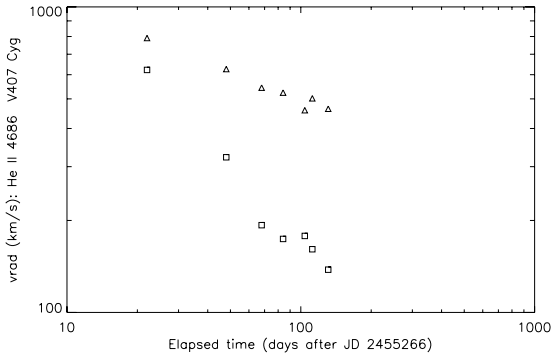

Fig. 27. Maximum positive (triangle) and negative (squares) radial velocities for He II 4686 Å from NOT spectra. A correction of 50 km s^{-1} has been applied to put the velocities in the rest frame of the red giant (see text for details).

propagating into the RG wind and the redshifted side displaying breakout of the ejecta. The terminal velocities can be fit with two power laws, the approaching side with an exponent of –0.84 ± 0.05 and the receding side with an exponent of –0.31±.05. After about day 90, the blue side of the profile changes more slowly and is consistent with the continued expansion of a stalled shock. Assuming an adiabatic shock in self-similar expansion (Sedov-Taylor) with a power law, and an ambient density varying as r^{-2} with distance r from the Mira (constant mass loss, constant terminal velocity), the blueshifted side that is propagating into the Mira wind follows a velocity scaling as $v \sim t^{-5/7}$ while the redshifted side should vary as $v \sim t^{-1/3}$. The highest ionization states (i.e. He^{+}, Ca^{+4}, Fe^{+6}, all of which have ionization potentials ≥54 eV) display line profiles that are nearly identical among themselves but essentially different from those with lower ionization potentials (i.e. N^{+}, O^{+}, Ar^{+2}, all ≤54 eV). In particular, the highest ionization species, Fe^{+6}, shows a third form for the line profile and also a systematic redshift. However, the blueward extension of the lines is asymptotically the same at around –200 km s^{-1} (i.e. ≈–150 km s^{-1} relative to the Mira). There are several possible explanations for the persistent blueward extension of the lines. One is the wake produced by the convergent shock on the rear side of the RG. This collimated structure is a generic feature of the explosion and seen in both the Walder et al. (2008) and Orlando et al. (2009) numerical simulations of the RS Oph outburst. The wake has a far longer lifetime than the shock crossing time and is maintained by the hot post-shocked gas expanding from the cavity generated within the RG wind. The alternate, more prosaic, explanation is that the approaching side of the shock passed through the denser inner parts of the wind and continued to expand at constant velocity within the increasingly rarefied parts of the RG wind. The Balmer lines were more symmetric and consistent with emission from the entire shock front, while the highest ionization lines show the strongest redward extension and can be explained as the receding portion of the bubble (partly obscured by the Mira) from the low density outer wind. The lowest ionization species, especially O I and Na I, also displayed asymmetric profiles but with a less pronounced velocity ratio and lower velocities and can be accounted for as the recombintion in the cooling shock. The virtual absence of H I singlets relative to the triplets, and the broad lines observed on Na I, O I, and Si II in the post-shocked gas may indicate charge exchange effects in a thin shock. This is supported by the relatively late appearance of the neutral broad lines, at a stage after the asymmetric He II 4686 Å line appeared. Similar effects have been discussed in the context of the Cygnus Loop and other older supernova remnants (e.g. Leutengger et al. 2010). We will examine this in more detail in the next paper.

The similarity of the outburst of V407 Cyg to that of RS Oph is striking, notwithstanding the differences in the properties of the systems. In this case, modeling performed for RS Oph (e.g. Walder et al. 2008) can also serve for interpreting V407 Cyg. The explosion should have been non-spherical, although possibly less so than for the much shorter orbital period systems RS Oph and T CrB. Wind confinement toward the orbital plane may not be so developed in V407 Cyg as in the other two and it is plausible that the ejection was less collimated. Our simple line profile modeling of [Fe VII] supports this hypothesis. There is evidently neutral and weakly ionized material that has neither been highly ionized nor swept up in the shock. However, the disappearance of the narrow absorption lines on Hβ and the changes in the high ionization species' profiles suggests that substantial acceleration has taken place in the ambient matter. Numerical simulations (Walder et al. 2008) displayed a near doubling of the ejecta mass through mixing with the wind as the shock traverses this ambient medium within the first week. In the V407 Cyg system this may be longer.

As to the binary system itself, some quantitative constraints can be placed based on the similarity to RS Oph and the properties of the RG. The Mira has a long pulsation period and based on the Munari et al. (1990) radius, 400 $R_{\odot}$, it must not be filling its Roche surface. If the strong Li I line is evidence of hot bottom burning, as argued by Tatarnikova et al. (2003b) (see also Herwig 2005 for a general review), then its mass must be greater than 4 $M_{\odot}$. Assuming that the WD is as massive as in RS Oph, around 1.2 $M_{\odot}$, then using the scaling from Eggleton (1983) for the ratio of the Roche radius, $R_{\rm RL}$, to the semimajor axis, a, gives $R_{\rm RL}/a \approx 0.3$ for a mass ratio of ≥3. If $R_{\rm RL} > R_{\rm Mira}$, then $a \geq 6$ AU, consistent with the *Fermi* γ-ray detection at 3 days after optical outburst (Abdo et al. 2010) for a shock velocity of around 2500 km s^{-1}. The period would therefore be long, as suggested by Munari et al. (1990), $P_{\rm orb} \geq 32$ yrs. This is a far longer orbital period than either RS Oph (Brandi et al. 2009) or T CrB, neither of which hosts a pulsating companion to the WD, and supports the conclusion that the degenerates in the symbiotic-like recurrent novae are the most massive among the symbiotic binaries[4].

Acknowledgements. P.K. was supported by ESA PECS grant No 98058. GMW acknowledges support from NASA grant NNG06GJ29G. A.P.B., J.P.O. & K.L.P. acknowledge the support of STFC. We thank C.-C. Cheung, J. Josè, K. Mukai, U. Munari, Quillo, and C. Rossi for discussions. We also thank the (anonymous) referee for helpful suggestions. S.N.S. acknowledges support from the PhD School "Galileo Galilei", Univ. of Pisa. Special thanks J. Mikolajewska for valuable discussions of this and related systems during her visit to Pisa in May 2010, and the *Fermi* LAT group (INFN-Pisa) for collaboration. Some spectra at Ondrejov were taken by L. Kotková , P. Škoda, and J. Polster. We have made extensive use of the Astrophysics Data System (ADS), SIMBAD (CDS), and the MAST archive (STScI) in the course of this work.

References

Abdo, A. A., Ackermann, M., Ajello, M., et al. 2010, Science, 329, 817
Anupama, G. C. 2008, in RS Ophiuchi (2006) and the Recurrent Nova Phenomenon, ed. A. Evans, M. F. Bode, T. J. O'Brien, & M. J. Darnley, ASP Conf Ser., 401, 31

[4] The referee pointed us to a study of RX Pup by Mikolajewska et al. (2002) that finds similarities between that system and both RS Oph and T CrB but with a longer period Mira variable (578 days) and a likely very long orbital period (>200 yrs). The line profile and photometric variations also show symbiotic nova-like outbursts similar to those observed in the 1930's in V407 Cyg. No explosive ejection has been detected from RX Pup but, in light of the noted similarities, it is worth monitoring.

Anupama, G. C., & Prabhu, T. P. 1989, JApA, 10, 237
Anupama, G. C., & Sethi, S. 1994, MNRAS, 269, 105
Bagnulo, S., Jehin, E., Ledoux, C., et al. 2003, The Messenger, 114, 10
Bode, M. F., & Evans, N. 2008, Classical Novae: 2nd Ed. (Cambridge: Cambridge Univ. Press)
Bode, M. F. 2010, AN, 331, 160
Brandi, E., Quiroga, C., Mikolajewska, J., Ferrer, O. E., & Garcia, L. G. 2009, A&A, 497, 815
Burrows, D. N., Hill, J. E., Nousek, J. A., et al. 2005, SSRv, 120, 165
Eggleton, P. P. 1983, ApJ, 268, 368
Evans, A., Bode, M. F., O'Brien, T. J., & Darnley, M. J. 2008, RS Ophiuchi (2006) and the Recurrent Nova Phenomenon, ASP Conf. 401
Gehrels, N., Chincarini, G., Giommi, P., et al. 2004, ApJ, 611, 1005
Gonzalez-Riestra, R. 1992, A&A, 265, 71
Herbig, G. H. 1975, ApJ, 196, 129
Herbig, G. H. 1988, ApJ, 331, 999
Hernanz, M., & José, J. 2008, NewAR, 52, 386
Herwig, F. 2005, ARA&A, 43, 435
Hoffmeister, C. 1949, VVS, 1, 295
IIjima, T. 2009, A&A, 505, 287
Jenniskens, P., & Desert, F.-X. 1994, A&AS, 106, 39
Kolotilov, E. A., Munari, U., Popova, A. A., et al. 1998, AstL, 24, 451
Kolotilov, E. A., Shenavrin, V. I., Shugarov, S. Yu., & Yudin, B. F. 2003, ARep, 47, 777
Leutengger, M. A., Beiersdorfer, P., Brown, G. V., et al. 2010, HEAD 11.1505
Meinunger, L. 1966, Mitteilunger über Veränderliche Sterne, Band 3, Heft 4
Mikolajewska, J. 2008, in RS Ophiuchi (2006) and the Recurrent Nova Phenomenon, ASP Conf. 401, 42
Mikolajewska, J., Brandi, E., Garcia, L., et al. 2002, AIPC, 637, 42
Munari, U., & Renzini, A. 1992, ApJ, 397, L87
Munari, U., Margoni, R., & Stagni, R. 1990, MNRAS, 242, 653
Munari, U., Siviero, A., & Valisa, P. 2010, ATel, 2546
Nishiyama, K., & Kabashima, F. 2010, CBET, #2199
Orlando, S., Drake, J. J., & Laming, J. M. 2009, A&A, 493, 1049
Patat, F., Chandra, P., Chevalier, R., et al. 2007, Science, 317, 924
Roming, P. W. A., Kennedy, T. E., Mason, K. O., et al. 2005, SSRv, 120, 95
Schmid, H.-M. 1996, MNRAS, 282, 511
Schmid, H. M., Krautter, J., Appenzeller, I., et al. 1999, A&A, 348, 950
Shaefer, B. E. 2010, ApJS, 187, 275
Shore, S. N. 2008, in RS Ophiuchi (2006) and the Recurrent Nova Phenomenon, ed. A. Evans, M. F. Bode, T. J. OBrien, & M. J. Darnley, ASP Conf Ser., 401, 19
Shore, S. N., & Wahlgren, G. M. 2010, A&A, 515, A108
Shore, S. N., Sonneborn, G., Starrfield, S., et al. 1993, AJ, 106, 2408
Shore, S. N., Kenyon, S. J., Starrfield, S., & Sonneborn, G. 1996, ApJ, 456, 717
Shugarov, S. Yu., Tatarnikova, A. A., Kolotilov, E. A., et al. 2007, BaltA, 16, 23
Simon, J. D., Gal-Yam, A., Gnat, O., et al. 2009, ApJ, 702, 1157
Sokoloski, J. L., Luna, G. J. M., Mukai, K., & Kenyon, S. J. 2006, Nature, 442, 276
Starrfield, S. 2008, in RS Ophiuchi (2006) and the Recurrent Nova Phenomenon, ed. A. Evans, M. F. Bode, T. J. O'Brien, & M. J. Darnley, ASP Conf Ser., 401, 4
Tatarnikova, A. A., Marrese, P. M., Munari, U., et al. 2003a, AstrL, 29, 405
Tatarnikova, A. A. Marrese, P. M., Munari, U., et al. 2003b, MNRAS, 344, 1233
Walder, R., Folini, D., & Shore, S. N. 2008, A&A, 484, L9
Wilms, J., Allen, A., & McCray, R. 2000, ApJ, 542, 914
Wilson, R. E. 1953, GCRV (Carnegie Inst. Wash. Pub. 601)